HHS Public Access

Author manuscript

Nat Nanotechnol. Author manuscript; available in PMC 2018 August 16.

Published in final edited form as:

Nat Nanotechnol. 2016 November ; 11(11): 941–947. doi:10.1038/nnano.2016.137.

Magneto-aerotactic bacteria deliver drug-containing nanoliposomes to tumour hypoxic regions

Ouajdi Felfoul[1,*], **Mahmood Mohammadi**[1,*], **Samira Taherkhani**[1,7,*], **Dominic de Lanauze**[1], **Yong Zhong Xu**[6], **Dumitru Loghin**[1], **Sherief Essa**[4,7], **Sylwia Jancik**[6], **Daniel Houle**[6], **Michel Lafleur**[4], **Louis Gaboury**[5], **Maryam Tabrizian**[7,8], **Neila Kaou**[1], **Michael Atkin**[1], **Té Vuong**[2], **Gerald Batist**[2], **Nicole Beauchemin**[3], **Danuta Radzioch**[6,*], and **Sylvain Martel**[1,&]

[1]NanoRobotics Laboratory, Dept. of Computer and Software Eng., Inst. of Biomedical Eng., Polytechnique Montréal, Montréal, Canada

[2]Segal Cancer Centre, Jewish General Hospital, Dept. of Oncology, McGill University, Montréal, Canada

[3]Rosalind and Morris Goodman Cancer Research Centre, Dept. of Biochemistry, Medicine and Oncology, McGill University, Montréal, Canada

[4]Dept. of Chemistry, University of Montréal (UdM), Montréal, Canada

[5]Institute for Research in Immunology and Cancer (IRIC), Dept. of Pathology and Cell Biology, University of Montréal, Montréal, Canada

[6]McGill University Health Centre, Montréal, Canada

[7]Dept. of Biomedical Eng., McGill University, Montréal, Canada

[8]Faculty of Dentistry, McGill University, Montréal, Canada

Abstract

Oxygen depleted hypoxic regions in the tumour are generally resistant to therapies[1]. Although nanocarriers have been used to deliver drugs, the targeting ratios have been very low. Here, we

[&]Corresponding author (sylvain.martel@polymtl.ca).
[*]These authors contributed equally to this work

Author contributions

SM acted as principal investigator, wrote the paper with the assistance from OF, MM, DR, ST, NB; and developed the general principles and methods. GB and TV provided clinical insights. OF, MM, ST, YZX, DdL, DL, DH performed the experiments with tumor-bearing animals. SJ, YZX and DH did the iv injections, processed all blood and tissues for analysis and made the analysis of the samples. LG performed immunohistochemistry, immunofluorescence and histopathological evaluations. NK, MM assisted by MA acted as project managers. MM and OF performed the experiments for the preliminary *in vivo* proof-of-concepts. OF designed the experimental platform. DdL tested the magnetotactic control process, which was executed by DL. ML and SE synthesized the liposomes. MT and ST attached the liposomes to the MC-1 cells. MM cultivated and prepared the bacteria for injection. MM, DR, GB, LG, NB and SM made the revisions of the manuscript and figures. YZX and DH coordinated the implantations of tumour xenografts. DL developed and calibrated the MC-1 counting software.

Additional information

Supplementary information accompanies this paper at www.nature.com/naturenanotechnology.

Competing financial interests

The authors declare no competing financial interests.

show that the magneto-aerotactic migration behaviour[2] of magnetotactic bacteria[3], *Magnetococcus marinus* strain MC-1[4], can be used to transport drug-loaded nanoliposomes into hypoxic regions of the tumour. In their natural environment, MC-1 cells, each containing a chain of magnetic iron-oxide nanocrystals[5], tend to swim along local magnetic field lines and towards low oxygen concentrations[6] based on a two-state aerotactic sensing system[2]. We show that when MC-1 cells bearing covalently bound drug-containing nanoliposomes were injected near the tumour in SCID Beige mice and magnetically guided, up to 55% of MC-1 cells penetrated into hypoxic regions of HCT116 colorectal xenografts. Approximately 70 drug-loaded nanoliposomes were attached to each MC-1 cell. Our results suggest that harnessing swarms of microorganisms exhibiting magneto-aerotactic behaviour can significantly improve the therapeutic index of various nanocarriers in tumour hypoxic regions.

Oxygen consumption by the rapidly proliferative tumour cells results in approximately < 0.7% O_2-depleted tumour areas that are known as hypoxic regions[7]. Currently used pharmaceutical nanocarriers such as liposomes, micelles, polymeric nanoparticles and many others, generally fail to reach these hypoxic regions[8]. Combining the enhanced permeability and retention (EPR) effect of nanocarriers with the longer systemic circulation properties achieved following PEGylation has increased the targeting ratio, but still results in a very limited fraction of nanocarriers entering tumours. Since only 5% of the administered nanocarriers remain in the systemic circulation after 12 h, this ultimately results in ~2% of the total administered dose being deposited in the tumour[9].

The main targeting limitations of these nanocarriers are their reliance on systemic circulation, the lack of a propelling force to penetrate the tumour beyond their diffusion limits[10], and the absence of sensory-based displacement capability to target the hypoxic zones. Although robotic functionalities could correct for such deficiencies, scaling issues have prevented their integration into an artificial carrier. Therefore, harnessing a natural agent with the proper characteristics and functionalities was considered instead.

One example is the *Magnetococcus marinus* strain MC-1. In their natural environment, MC-1 cells rely on geomagnetic-assisted aerotaxis known as magneto-aerotaxis to efficiently migrate to and maintain position at preferred low oxygen concentrations at the oxic-anoxic transition zone (OATZ).

Our hypothesis was that a similar OATZ present in the tumour interstitium between the angiogenic network (oxic) and the tumour necrotic (anoxic) zones could be exploited to enhance drug targeting to hypoxic regions using live MC-1 cells being guided by an external magnetic source. Indeed, unlike previous bacterial therapies[11], minimizing systemic circulation of drug-loaded MC-1 cells was achieved by initially guiding them (see Methods: magnetotaxis directional control) towards such OATZ where oxygen gradients could be detected by the bacteria. Magnetotaxis was first prioritized over aerotaxis since, unlike hypoxic zones, the location of a tumour mass can generally be precisely determined.

Based on the Langevin function, the level of magnetotactic directional control characterized by the alignment of the MC-1 membranous chain of Fe_3O_4 nanoparticles known as magnetosomes[12] in the applied directional magnetic field depends on the ratio of the

interactive magnetic energy with the applied field to the thermal energy. Without a magnetic field, thermal forces associated with Brownian motions randomize the cell orientation unless the MC-1 detects an oxygen gradient in the tumour interstitium. Therefore, we first used a 3D targeting magnetic field slightly higher than the geomagnetic field to induce a stronger directional torque on the chain of magnetosomes[13] to penetrate the tumour from the peritumoral regions. This was followed by a MC-1 autonomous aerotactic directional phase when the bacteria penetrated the tumour. The physiological environments encountered by the MC-1 were different from the ones found along their natural migrating paths; thus, the experiments were aimed at assessing whether the MC-1 cells would effectively migrate towards the hypoxic zones following a peritumoral injection. More specifically, we questioned whether the spherical MC-1 cells (diameter of 1–2 μm) would be able to migrate through potential delivery routes such as the irregular and disorganized angiogenic network, the interstitial spaces, and the intercellular openings of less than 2 μm between endothelial cells[14] within solid tumours.

The antibodies used for the detection of MC-1 receptors were custom made. Their specificity has been demonstrated in this study using xenografts injected with either PBS or MC-1 (Fig. 1) and using *H. pylori* as a negative control (Supplementary Fig. 1). To better visualize the hypoxic tumour regions and demonstrate co-localization of the bacteria, we injected a hypoxia-specific hydroxyprobe prior to tumour excision (see Methods: staining of the hypoxic regions). The results, illustrated in Fig. 2a, b, (see also Supplementary Fig. 2) clearly demonstrated co-staining of MC-1 bacteria (FITC staining, Supplementary Fig. 2A panel c) and hypoxic regions labelled in brown (Supplementary Fig. 2A panels a and b; see also Methods: immunohistology staining). To further confirm the identity of the previously detected MC-1 in tumour sections (see Methods: digitization of transverse tumour sections), several sections were also analysed using electron microscopy (for details on samples preparation, see Methods: transmission electron microscopy). One representative section depicted in Fig. 2, panel d, shows magnetosomes inside a MC-1 cell.

To assess magnetically-guided live MC-1 (for bacteria preparation before injection, see Methods) in HCT116 xenografts (for details on the preparation of HCT116 tumour cells, see Methods), we peritumorally injected 20 mice with ~5×10^7 bacteria in 50 μl of PBS solution. Depending on whether or not a magnetic field was applied to directionally guide the bacteria, two groups were present, namely an experimental group (group I) submitted to a 30 min directional magnetic field using a specially made platform dubbed the magnetotaxis system (Fig. 3a) targeting the xenograft (Fig. 3b); and a control group (group II) not exposed to the magnetic field. Colour superimposition shows MC-1 distribution in the xenograft of group I mice (Fig. 3c) or group II mice (Fig. 3d). The results for both groups are shown in 4 transverse 5×5 mm^2 sections, 2, 4, 6, and 8 mm from the injection site in the magnetically targeted corridor passing through the centre of the tumour.

Total number of MC-1 for each section along the central longitudinal axis of the tumour is depicted in Fig. 3e. Many more MC-1 cells were detected in group I tumours. Independently of the distance from the injection site, Fig. 3f defines the total number of injected or detected MC-1 cells for each group. Total number of directionally-guided MC-1 significantly outnumbers those not exposed to the magnetic field. This result demonstrates the importance

of the directional magnetic field to achieve deep MC-1 penetration and distribution inside the tumour.

The targeting profile was further compared with two types of passive agents, i.e. agents lacking the three functionalities previously mentioned namely, magnetotactic guidance, propelling force, and sensory-based displacement. The first passive agent consisted of polymer microspheres (PS) and the second being dead MC-1 cells (see Methods: live/dead mixture preparation) having undergone prior staining with a fluorescent cell penetrating peptide (CellTrace, CFSE Cell Proliferation Kit). When such passive agents are injected in the peritumoral region, they exhibit a limited diffusion, likely due to the tumour interstitial fluid pressure[15]. The simultaneous peritumoral injection of live MC-1 with these passive agents was performed to compare their ability to diffuse and remain inside the tumour under the same experimental conditions. 20 μl of Dragon green fluorescent PS (480, 520) 1.9 μm, similar in size to the MC-1 spherical cells, and 20 μl of live MC-1 were injected. This consisted of ~2.92×10^7 bacteria and ~1.35×10^7 beads, followed by 30 min of magnetic guidance. In a separate set of experiments, 20 μl of dead MC-1 were used instead of the polymer microspheres. Texas Red labelled secondary antibody was coupled to MC-1 staining the live MC-1 in red with the beads alone in green. The dead MC-1 cells appear yellow.

The active directional motility through magnetotaxis and aerotaxis of the MC-1 resulted in superior penetration depths in HCT116 xenografts compared to passive agents as depicted by the dead MC-1 and the polymeric beads (Fig. 4, a–c). We observed a substantial decrease in the number of microspheres as sections were produced from deeper regions of the tumour, while the number of live MC-1 increased significantly (Fig. 4b). The co-localization of live MC-1-bead complexes (Fig. 4d) that occurred from the surface interaction of some beads with MC-1 suggests the potential for each MC-1 to carry a large payload deeply inside tumoral tissues. Similarly, live MC-1 cells located further away from the injection site and deeper into the tumour outnumbered dead MC-1 cells (Fig. 4e). The injection site exhibited a strong passive diffusion of the CellTrace making the background fluorescent in which mostly dead MC-1 (yellow dots) and few live MC-1 (red dots) were found.

To evaluate the mean targeting ratio of MC-1 with covalently-attached[16] (see also Methods: liposome attachment) SN-38 drug-loaded liposomes (MC-1-LP) (Fig. 5a), we conducted additional *in vivo* experiments in HCT116-injected SCID Beige mice. Among all potential nanocarriers, liposomes were initially selected as a first proof-of-concept because they are biocompatible, exhibit low immunogenicity and high flexibility, and protect the body from potential toxic cargo. Liposomes also shield therapeutic agents from premature degradation, control release kinetics, and may encapsulate a multitude of hydrophilic and/or hydrophobic drug cargos, pharmaceutical ingredients, imaging agents, and genetic material by virtue of their aqueous interior and lipid exterior. Furthermore, cytotoxicity assays revealed that liposomal attachments to the MC-1 formulation improved the biocompatibility of the MC-1 and attachment did not interfere with liposomal uptake[16]. The diameter of each liposome was set to its optimal value of ~170 nm to maximize the quantity of drug-cargo being transported per MC-1 cell.

Similar to the results achieved with the unloaded MC-1 (Fig. 3), high targeting ratios of MC-1-LP (Fig. 5b) were obtained. Histological sections of the samples also revealed that the MC-1-LP were distributed throughout the xenografts (Fig. 5, c and d) mainly in the neighbourhoods of hypoxic and necrotic areas, and in large numbers in the centre of the tumour where necrosis and hypoxic regions predominated. The mean tumour targeting ratio (>50%) was first estimated from the samples by image processing techniques (see Methods: MC-1 count), allowing assessment of the distribution of the MC-1-LP complexes in the HCT116 xenografts. After excision of the tumours, HCT116 xenografts were also homogenized to evaluate and to confirm the number of MC-1 bacteria (Fig. 5b).

Live MC-1 cells that could prove to be clinically safe (see Methods: cytotoxicity assays in mice and rats, and Supplementary Fig. 3 and Fig. 4) could be used as direct targeting vectors (i.e. vectors that reach the target using the shortest physiological routes) to enhance the therapeutic index while reducing systemic exposure in currently used passive and active targeting methods[17]. Besides targeted chemotherapy, many other therapeutic modalities could benefit from such a delivery method including but not limited to radiotherapeutic treatments[18] that could be enhanced by radio-sensitizers being delivered in the tumour hypoxic regions[19]. Combining magnetotactic guidance that relies on a weaker magnetic field independent of the MC-1 population (i.e. while maintaining the magnetic field strength constant, dosages can be increased using swarms that can largely exceed the ~100 million drug-loaded MC-1 cells per injection used for this study - Fig. 5b) with the self-propelling force of the MC-1, would allow magnetic targeting[20] at any depth within a human adult unlike magnetic nanoparticles and carriers[21] that are limited by fast decays of induced forces with distances from the magnetization sources. Depth-independent direct delivery methods such as magnetic resonance navigation[22] cannot be effectively applied to tumoral microenvironments due to the insufficient magnetic induction volume of the agents. Although microscopic artificial swimmers[23] could be envisioned as an alternative to the use of natural microorganisms, embedding an equivalent level of functionality in artificial agents to compete against such natural microorganisms in delivering therapeutics effectively to tumour hypoxic regions may prove to be a far-reaching concept.

Indeed, we showed the possibility to harness sufficiently small microorganisms exhibiting magneto-aerotactic behaviours, such as the MC-1 cells, that essentially function as an agent with oxygen gradient detectors connected to a low Reynolds hydrodynamic propelling system through some sort of embedded computation or intelligence, all in < 2 μm self-powered body capable of being directionally guided from an external source. When operating in a computer-controlled magnetic environment, such microorganisms can emulate artificial medical nanorobots or transporters that need characteristics and functionalities well beyond actual technological feasibility. Furthermore, such an approach could also benefit from the fact that bacteria-mediated delivery of nanoparticles and cargo into cells for various applications is already feasible[24]. Besides potential future efforts towards genetically modified carriers[25] based on known genome sequences[26] and the development of better magnetotactic guidance algorithms to increase the therapeutic index further, these initial findings may influence not only specific engineering concepts and medical interventional methods, but also open opportunities for the synthesis of new targeted therapeutic, imaging,

and diagnostic vectors while providing further opportunities to enhance the delivery and efficacy of existing nanocarriers.

METHODS

Magnetotaxis directional control

Each animal was placed in the centre of a custom-made platform being referred to as the magnetotaxis system. Although several configurations of the magnetotaxis system are possible, the version of the platform used for the experimentations consisted of three orthogonal pairs of electric coils positioned in a Maxwell configuration as depicted in Fig. 3a. A directional magnetic field generated by the magnetotaxis platform was applied towards the xenograft in order to guide the bacteria through the centre of the tumour. A focalized directional magnetic field of only ~15 Gauss was applied for a predetermined period of 30 min (although much less than 30 min may be required for targeting) before being switched off to allow aerotaxis (aerotactic displacement of the MC-1) to take effect.

Staining of the hypoxic regions

The hydroxyprobe reaction was carried out according to the manufacturer's protocol. Briefly, Hypoxyprobe-1 Omni kit (Hypoxyprobe, Inc. PAb2627AP, 1/200) was applied on every sample at room temperature for 60 min. Sections were then incubated with a specific secondary anti-rabbit biotin conjugated for 32 min at room temperature. Finally, sections were counterstained with Hematoxylin and Bluing reagent for 4 min each (Ventana Medical Systems, Roche, Tucson, AZ).

Immunohistology staining

Samples were fixed in 10% neutral buffer formalin, embedded in paraffin and sectioned at 4 μm. Labelling reactions (IHC or IF) were carried out in an automated immunostainer (Discovery XT, Ventana Medical Systems, Roche Group) using proprietary reagents. The following antibodies were applied: Polyclonal Rabbit anti-MC1 receptor (dilution 1/300 for 1 h at room temperature). Afterwards, the slides were incubated with a FITC-labelled secondary anti-rabbit antibody to visualize the MC-1 receptor in green. A Texas Red-labelled secondary anti-rabbit antibody was used to visualize the MC-1 receptor in red. The slides were finally washed and mounted using ProLong® Gold Antifade Reagent with DAPI (Invitrogen).

Digitization of transverse tumour sections

Tumours were paraffin-embedded and serially sectioned. Transverse tumour sections were scanned at 40× magnification on a Nanozoomer 2HT (Hamamatsu) equipped for bright field and fluorescence acquisition (triple filter cube DAPI/FITC/TxRed) or images of each section were acquired using a fluorescence optical microscope equipped with magnification objective lens.

Transmission electron microscopy (TEM)

Representative portions of the paraffin-embedded sections were reprocessed for transmission electron microscopy (TEM). Briefly, fragments of interest were dissected out of the paraffin blocks and reprocessed. The following steps were carried out including dewaxing, rehydration, post-fixation in OsO_4 (Osmium tetraoxyde) dehydration and embedding in Epon 812. Ultrathin sections of OsO_4 blocks were carried out using a Reichert S Ultramicrotome and mounted on copper naked grids. Sections were contrasted with uranyl acetate and lead citrate before being examined using a Philips CM100 electron microscope and digital micrographs captured using an AMT XR80 CCD digital camera.

Bacteria preparation before injection

The composition of the culture medium has been described previously (see ref. 16). At the end of the exponential phase and before the beginning of the stationary phase, 50 ml of ~2×10^6 MC-1 cells per ml were purified and washed three times in PBS by applying a 2D magnetic field prior to being re-suspended in 100 μl PBS (pH=7.4).

Preparation of HCT116 tumour cells

HCT116 cell line was purchased from Horizon Discovery Ltd. (www.horizondiscovery.com) and maintained in McCoy's 5A medium (Multicell) supplemented with 10% FBS and 1% penicillin/streptomycin at 37°C in a 5% CO_2 incubator. HCT 116 cells are routinely tested for Mycoplasma and have been confirmed to be negative for Mycoplasma sp. infection. Two days prior to implantation, cells were divided into flasks with fresh growth medium. Cells were harvested from the flasks by using 0.05% trypsin-EDTA solution and collected by centrifuge at 450 × g for 5 min. Cells were washed once with PBS and were re-suspended in PBS at a final concentration of 5×10^7 cells/ml. For establishing the tumour xenograft model, 100 μl of the cell suspension were subcutaneously injected into the left flank of SCID-beige mice (Charles River). Less than 5% of the animals (1 in 20 mice injected with HCT116 cells) occasionally displayed exceptionally slow growth of the tumour. These animals were excluded from the study. The two experimental groups (experimental group subjected to a magnetic field and the control group unexposed to the magnetic field) were randomized following measurement of the tumour sizes. All groups had similar (no statistically significant difference) average tumour sizes at the start of the experiment.

Live/dead mixture preparation

A cell pellet of live MC-1 was obtained by magnetically concentrating 50 ml of a MC-1 solution. The pellet was suspended in PBS containing the probe prepared as suggested by the manufacturer for 15 min at room temperature. The MC-1 were magnetically concentrated to reform the pellet and incubated for another 30 min at 42°C at which the MC-1 became inactive, assessed by microscopy observation. After heat treatment, the MC-1 did not recovered motility and cell division, also assessed by microscopy observation over the duration of the experiment.

Liposome attachment

The attachment relies on direct chemical conjugation of liposomes functionalized with reactive groups (–COOH) which covalently bind to primary amino groups ($–NH_2$) intrinsic to bacteria cell membrane proteins. Carboxylated liposomes were conjugated to MC-1 by carbodiimide chemistry. Dehydrated agents such as EDC and Sulfo-NHS were added to 3 ml of 0.5 mM liposomes suspension (EDC: NHS: DSPE-PEG-COOH = 35:35:3, molar ratio) in PBS buffer (pH 6.5). The mixture was incubated at room temperature for 20 min. The free activating reagents were removed using Sephadex G-50 column. Then, activated liposomes were added to 50 ml of ~2×10^6 MC-1 cells per ml and incubated for 2 h at room temperature, under gentle mixing. Liposomes attached to MC-1 were separated from non-attached liposomes by applying a 2D magnetic field. The sample was washed three times in PBS and finally re-suspended in PBS (pH=7.4).

MC-1 count

To visualize and estimate the relative amounts of MC-1 present in histological sections sampled from tumours, images of each section were acquired using a fluorescence optical microscope equipped with a 40× magnification objective lens or the transverse tumour sections were scanned at 40× magnification. The acquired images were then processed using an automated software algorithm to evaluate the number of MC-1 in each histological section. This algorithm performed graphical enhancements on each image to count the number of MC-1. First, morphological erosion and dilation using a large disk shaped structural element was performed to remove noise resulting from non-uniformed lighting in the setup and subtracting the result of this operation from the original image. Second, pixels were classified as belonging to MC-1 cells or tumour background. Pixels classified as belonging to MC-1 cells needed to satisfy two conditions; first, the hue of the pixel as part of the HSV colour space needed to be in the range of hues which represent the bacteria in the histologic image; second, the intensity (lightness value) of the pixel as part of the HSV colour space, needed to be superior than a specific threshold of the bacteria appearing in the image. The total number of MC-1 cells in the tumour section was calculated by dividing the total number of MC-1 cells pixels by the average MC-1 cell size. This average MC-1 cell size was determined by summing the MC-1 cell classified pixels for 50 sample areas in which only one MC-1 cell was present. MC-1 cell distribution shown in Fig 3c and d were obtained by clustering the classified pixels in super-pixels. All super-pixels have the size of 128×128 pixels (844.25 μm^2), and their intensities are given by the total number of MC-1 cells classified pixels forming the super-pixel.

To ensure the reliability of the counting software, five different sections in each tumour were randomly selected and the bacteria in these sections were manually counted under microscopy observation, and compared to the results obtained by the software-based image processing techniques. The results showed negligible variations between the software-based and the manual counting methods.

In order to study the penetration of live MC-1 cells with and without magnetic field exposure, the total number of MC-1 cells for all tumour sections located at the same distance from the injection site for each of the two groups was summed (in total, there were 10

tumour xenografts/group and each xenograft was cut at 2, 4, 6 and 8 mm from the injection site). Fig. 3c, d, e represents the total number of MC-1 cells for each group at a given distance from the injection site. Fig. 3f represents the numbers of MC-1 in each tumor which were estimated using the equations found by the linear interpolation between each adjacent and actual data points.

In order to generate plots for the MC-1-LP distribution inside the tumor shown in Fig 5d, the numbers of MC-1 cells were plotted against the depth at which the sample was taken in the tumour. The amount of MC-1 in each tumor was estimated by adding together the number of MC-1 corresponding to every sample taken at a certain depth inside the tumour with a step of 2 mm between each value of depth from the first histological section's position to the last position. The curve's data for each 2 mm step were calculated using the equations found by the linear interpolation between each adjacent and actual data points.

Once the animals were randomized into two different groups, the processing of the samples and the analysis was performed using their unique ID number that did not identified the experimental group to which they belonged. Group assignments of each animal were revealed for statistical analyses.

For each injection, a bacterial sample was counted as a reference. Since some of the peritumorally-injected bacteria might not have penetrated the tumour, we estimated the percentage of bacteria found in the excised tumours. Some of the injected bacteria might have been dead and/or partly cleared from the tumour tissue, so the counts obtained represent only estimates for comparative purposes.

Code availability

The code used for counting the MC-1 cells is available at github.com (https://github.com/loghindo/NDPI_counting_MC1_bacteria).

Cytotoxicity assays in mice and rats

For the systemic response to MC-1 cells, no significant differences in the expression of inflammatory cytokines between PBS and MC-1 injections both in A/J and in C57BL6 mice in the blood were observed. *Pseudomonas aeruginosa* used as a positive control without MC-1 injection induced inflammatory cytokines, IL-6 being induced at the highest level after 6 h. Immunogenicity and organ toxicity assessments were also conducted. Immunogenicity studies were performed using various doses of MC-1 and harvesting blood as well as organs at various time points post i.v. infusion of MC-1 bacteria into two different strains of mice, the A/J and C57BL/6 strains. Following i.v. injection with *P.aeruginosa*, blood plasma displayed the highest levels of inflammatory cytokines compared to liver, spleen, and lungs. MC-1 did not induce significant increases in inflammatory cytokine levels in the liver, spleen, lungs as well as in the plasma. Rats were injected with 10^8 MC-1 intravenously and the complete biochemical and hematological assessments were performed after 6, 24 and 72 hrs. Our preliminary results demonstrated that the injection of MC-1 did not lead to inflammation, as no changes in blood counts were detected and biochemical parameters were within normal range (Supplementary Fig. 3 and Fig. 4).

Mice

The mice (all males) used in this study were SCID Beige (Charles River ®). The mice were 8 weeks old and weighed approximately 22 g. All the animals were pathogen free, murine virus free, *Helicobacter* and parasite-free. These animals were housed (1–4 animals/cage), and maintained in a barrier facility unit under specific pathogen-free conditions with a 12-hrs light/dark cycle, at 22°C ± 2 and at 50% ± 5 humidity. The animals were kept in polycarbonate (Lab Products®, Maywood New Jersey, USA) micro-isolator cages with sterile corn bedding (Harland Sprague Dawley - Catalogue No 7097 ®, USA) and maintained in ventilated rack, (Lab Products®, Maywood, New Jersey, USA)) with a cycle of 50 changes of fresh HEPA filter air per hour in each cage. The mice were fed with the NIH-31 modified mouse irradiated diet (Harlan Teklad®, Indianapolis, Indiana, USA). All mice had *ad libidum* access to food and sterile acidified water at pH 2.5.

Our animal protocol was reviewed and approved by the university facility animal care committees of the Montréal General Hospital and Glen Institute. Our protocol is in compliance with the Canadian Council for Animal Care (CCAC).

A statistician was consulted for selecting the appropriate statistical tests. The assumptions were made based on the pilot study results which showed normal distribution among all animals. The animals assigned to each of the groups (experimental and control groups) were selected so that no statistical difference in the starting average tumour size was observed between the groups.

Supplementary Material

Refer to Web version on PubMed Central for supplementary material.

Acknowledgments

This project was initially supported in part by the Canada Research Chair (CRC) Tier 2 in Micro/Nanosystem Development, Fabrication and Validation and grants from the National Sciences and Engineering Research Council of Canada (NSERC), and the Province of Québec. This work was primarily supported by the Québec Consortium for Drug Discovery (CQDM) and in part by the Research Chair of École Polytechnique in Nanorobotics, Mitacs, and later by the CRC Tier 1 in Medical Nanorobotics. The magnetotaxis system was built with the financial help of the Canada Foundation for Innovation (CFI). Preliminary *in vivo* results were obtained with the financial help of the US National Institute of Health (NIH) Grant Number R21EB007506 from the National Institute of Biomedical Imaging and Bioengineering. Judith Caron from CQDM is acknowledged for her involvement in the coordination of the project. Ronald Gladue from Pfizer Inc., Robert M. Garbaccio from Merk & Co., and Corinne Reimer from AstraZeneca R&D, are also acknowledged for their guidance and insights from the pharmaceutical industry. Charles C. Tremblay (NanoRobotics Lab.) helped in determining the number of bacteria in samples and Timothy John (Biomat'x, McGill U) in preparation of liposomes. Julie Hinsinger (UdM, IRIC) and the histological team (UdM, IRIC) are acknowledged for tumours histology preparation and Diane Gingras (UdM, IRIC) for transmission electron microscopy.

References

1. Vaupel P, Mayer A. Hypoxia in cancer: significance and impact on clinical outcome. Cancer Metastasis Rev. 2007; 26:225–239. [PubMed: 17440684]
2. Frankel RB, Bazylinski DA, Johnson MS, Taylor BL. Magneto-aerotaxis in marine coccoid bacteria. Biophys. J. 1997; 73:994–1000. [PubMed: 9251816]
3. Blakemore RP. Magnetotactic bacteria. Science. 1975; 190:377–379. [PubMed: 170679]

4. Bazilinski DA, et al. Magnetococcus marinus gen. nov., sp. nov., a marine, magnetotactic bacterium that represents a novel lineage (Magnetococcaceae fam. nov., Magnetococcales ord. nov.) at the base of the Alphaproteobacteria. Int J Syst Evol Microbiol. 2013; 63:801–808. [PubMed: 22581902]
5. Bazylinski DA, Frankel RB, Jannasch HW. Anaerobic magnetite production by a marine, magnetotactic bacterium. Nature. 1988; 334:518–519.
6. Lefèvre CT, et al. Diversity of magneto-aerotactic behaviors and oxygen sensing mechanisms in cultured magnetotactic bacteria. Biophys. J. 2014; 107:527–538. [PubMed: 25028894]
7. Brown JM, Wilson WR. Exploiting tumour hypoxia in cancer treatment. Nature Reviews. 2004; 4:437–446.
8. Wilson WR, Hay MP. Targeting hypoxia in cancer therapy. Nat Rev Cancer. 2011; 11(6):393–410. [PubMed: 21606941]
9. Hong M, Zhu S, Jiang Y, Tang G, Pei Y. Efficient tumor targeting of hydroxycamptothecin loaded PEGylated liposomes modified with transferrin. J. Control. Release. 2009; 133:96–102. [PubMed: 18840485]
10. Tannock IF, Lee CM, Tunggal JK, Cowan DSM, Egorin MJ. Limited penetration of anticancer drugs through tumor tissue. Clin. Cancer Res. 2002; 8:878–884. [PubMed: 11895922]
11. Patyar S, et al. Bacteria in cancer therapy: a novel experimental strategy. J. Biomed. Science. 2010; 17:21.
12. Schüler D. Formation of magnetosomes in magnetotactic bacteria. J. Molec. Microbiol Biotechnol. 1999; 1:79–86. [PubMed: 10941788]
13. de Lanauze D, Felfoul O, Turcot J-P, Mohammadi M, Martel S. Three-dimensional remote aggregation and steering of magnetotactic bacteria microrobots for drug delivery applications. Int. J. Robot. Res. 2014; 33(3):359–374.
14. McDonald DM, Baluk P. Significance of blood vessel leakiness in cancer. Cancer Res. 2002; 62:5381–5385. [PubMed: 12235011]
15. Heldin C-H, Rubin K, Pietras K, Ostman A. High interstitial fluid pressure-an obstacle in cancer therapy. Nat. Rev. Cancer. 2004; 4:806–813. [PubMed: 15510161]
16. Taherkhani S, Mohammadi M, Daoud J, Martel S, Tabrizian M. Covalent binding of nanoliposomes to the surface of magnetotactic bacteria acting as self-propelled target delivery agents. ACS Nano. 2014; 8:5049–5060. [PubMed: 24684397]
17. Préat V. To exploit the tumor microenvironment: Passive and active tumor targeting of nanocarriers for anti-cancer drug delivery. J. Controlled Release. 2010; 148:135–146.
18. Harrison LB, Chadha M, Hill RJ, Hu K, Shasha D. Impact of tumor hypoxia and anemia on radiation therapy outcomes. Oncologist. 2002; 7:492–508. [PubMed: 12490737]
19. Moeller BJ, Richardson RA, Dewhirst MW. Hypoxia and radiotherapy: Opportunities for improved outcomes in cancer treatment. Cancer Metastasis Rev. 2007; 26:241–248. [PubMed: 17440683]
20. Polyak B, Friedman G. Magnetic targeting for site-specific drug delivery: applications and clinical potential. Expert Opinion on Drug Delivery. 2009; 6:53–70. [PubMed: 19236208]
21. Rotariu O, Strachan NJC. Modelling magnetic carrier particle targeting in the tumor microvasculature for cancer treatment. J. Magnetism and Magnetic Materials. 2005; 293:639–646.
22. Martel S, et al. Automatic navigation of an untethered device in the artery of a living animal using a conventional clinical magnetic resonance imaging system. Appl. Phys. Lett. 2007; 90:114105.
23. Dreyfus R, et al. Microscopic artificial swimmers. Nature. 2005; 437:862–865. [PubMed: 16208366]
24. Akin D, et al. Bacteria-mediated delivery of nanoparticles and cargo into cells. Nature Nanotechn. 2007; 2:441–449.
25. Jain RK, Forbes NS. Can engineered bacteria help control cancer? Proc. Natl. Acad. Sci. 2001; 98:14748–14750. [PubMed: 11752416]
26. Schübbe S, et al. Complete genome sequence of the chemolithoautotrophic marine magnetotactic coccus strain MC-1. Appl. Environ. Microbiol. 2009; 75:4835–4852. [PubMed: 19465526]

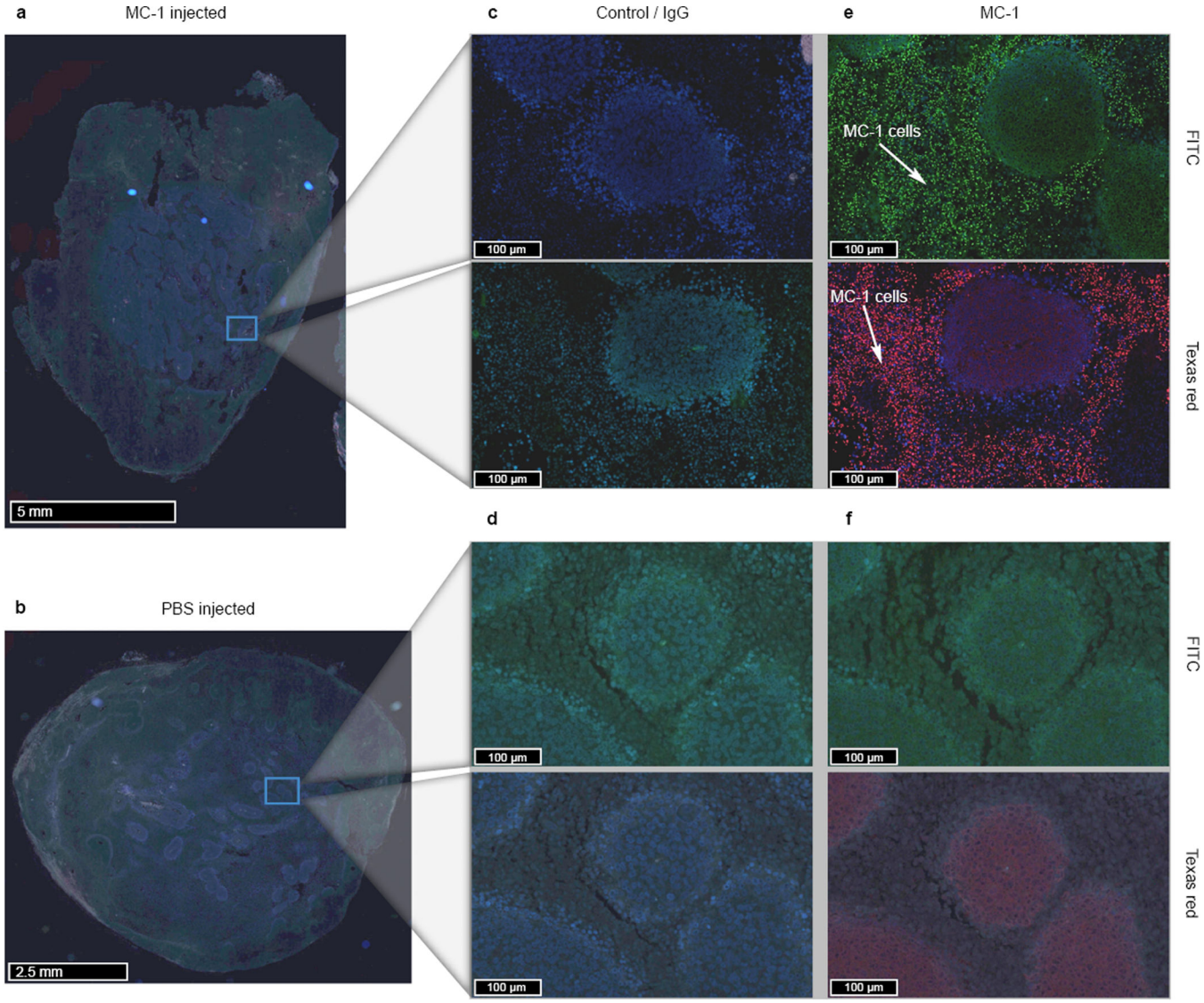

Figure 1. Assessment of the specificity of MC-1 antibody in HCT116 colorectal xenografts in SCID Beige mice

To ascertain specificity of MC-1 antibody, xenografts were injected with either MC-1 **(a)** or PBS **(b)**. An unrelated IgG isotype (6.6 µg/ml) was used (**c** and **d**) along with the Polyclonal Rabbit MC-1 antibody (**e** and **f**) on two adjacent sections of the same xenograft. In both cases, the reaction was revealed using either FITC (green) or Texas red (red) secondary antibodies. Specific labelling could be observed only in the MC-1 injected xenografts incubated with MC-1 antibody. Control IgG was unable to identify MC-1. These results confirmed the specificity of the antibodies to detect MC-1 cells in the tumours.

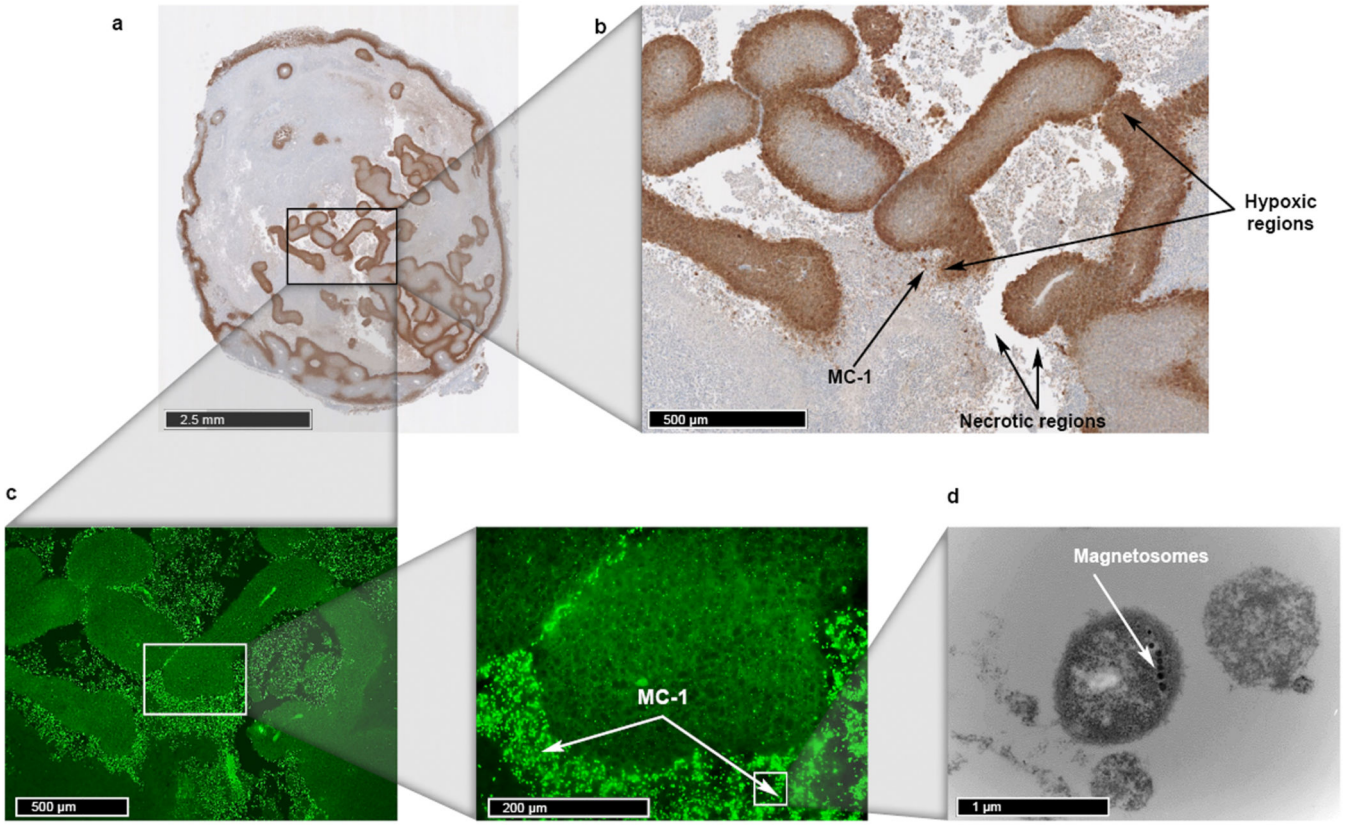

Figure 2. MC-1 cells are preferentially located in the hypoxic regions of the xenografts

To determine the exact location of MC-1 with regards to the local oxygen tension in tissue, a hypoxyprobe-specific antibody labelled with biotin was used, as illustrated in panels **a** and **b**, where strands and islands of remaining hypoxic tumour tissue give a positive brownish reaction in the vicinity of necrotic areas, as illustrated in panel **b**. The MC-1 antibodies specifically detect MC-1 that is visualized by staining with anti-rabbit FITC-labelled secondary antibodies (panel **c**, 10× and 40×). In panel **c**, the adjacent sections of the same xenografts were incubated with MC-1 antibody and a FITC-conjugated specific secondary antibody to label MC-1, thus confirming the presence of abundant bacteria in areas of lowered oxygen concentration (10× and 40× images of MC-1 FITC fluorescently-labelled), high-resolution images were acquired manually using a DP71 digital camera mounted on a Olympus BX61 motorized upright microscope with fluorescence (FITC/TXRED/DAPI). In panel **d**, a representative portion of a paraffin-embedded section reprocessed for transmission electron microscopy (TEM) is illustrated, to identify the MC-1 bacteria according to their typical ultra-structural features including presence of magnetosomes. The representative pictures were selected from stained sections obtained using 10 different tumours isolated from the 10 tumour-bearing mice collected in three independent experiments.

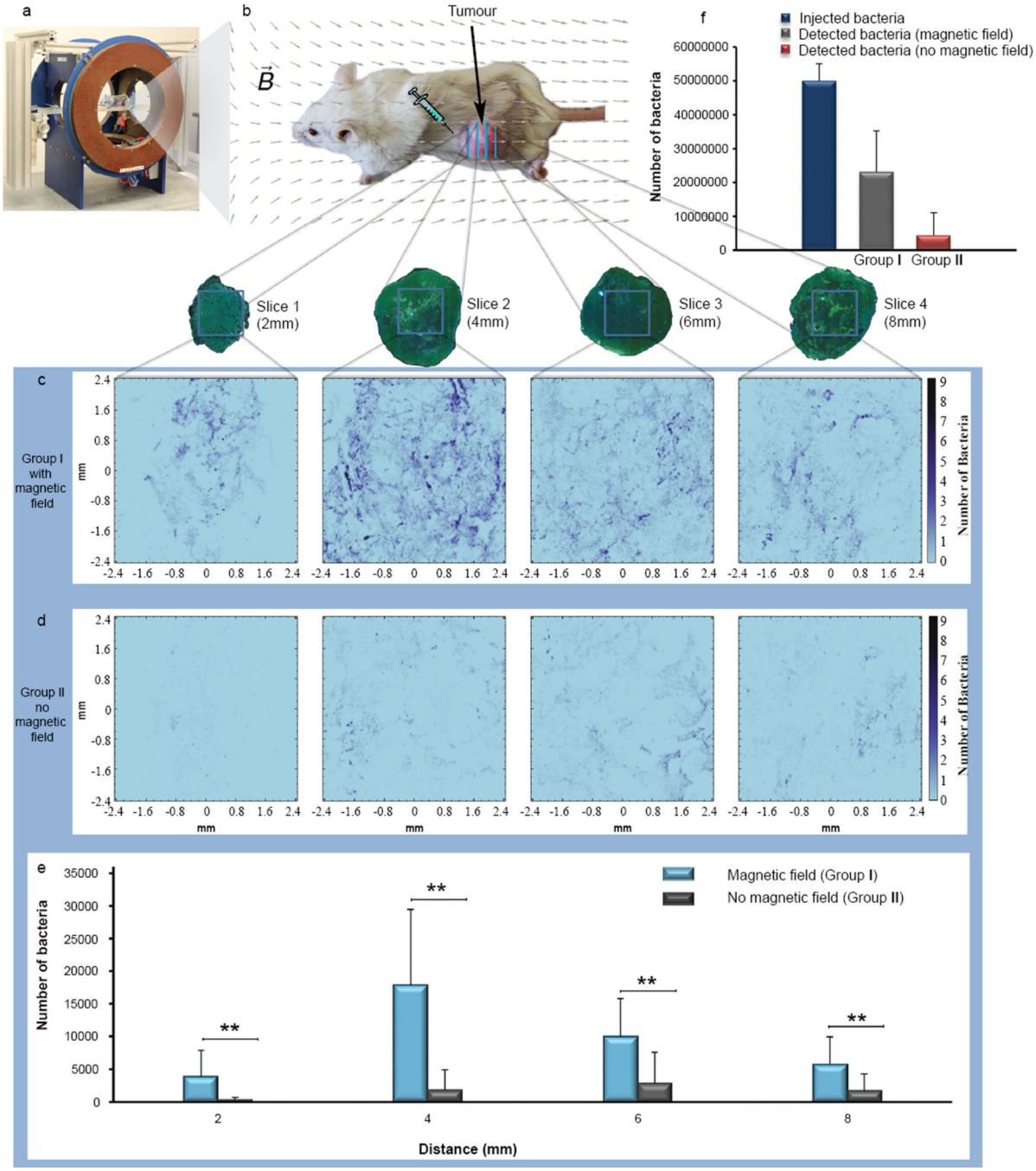

Figure 3. Penetration of live MC-1 with and without magnetic field exposure in HCT116 xenografts following a peritumoral injection

a, Magnetotaxis directional control system used to generate the magnetic field necessary to guide the MC-1 cells towards the xenograft. **b**, MC-1 peritumoral injection in HCT116 tumour xenograft in mice and representation of the applied directional magnetic field used in this study to direct the bacteria towards the xenograft. The directional magnetic field, $\vec{B}$ was aligned towards the centre of the tumoral volume. **c** and **d**, MC-1 average distribution in transverse tumour (n=10) sections visualized by staining with anti-rabbit FITC-labelled

secondary antibodies at 2, 4, 6 and 8 mm from the peritumoral injection site for **(c)** group I and **(d)** group II. The results show not only a significant increase of the targeting ratios of MC-1 cells that was magnetically-guided compared to non magnetically-guided MC-1, but also led to a good distribution in the tumoral volume and more specifically in the tumor hypoxic regions. The higher populations of MC-1 cells of group I contribute in targeting all hypoxic regions in the tumour. **e**, Standard deviation and average number of MC-1 for the transverse tumor sections in groups I and II. Statistical analysis was performed using unpaired t-student. Significant difference was considered for $^{**}P < 0.01$. The results clearly show a significant increase of MC-1 cells for group I in the tumoral volume where magnetotactic directional guidance was used prior to remove the magnetic field to enable aerotactic displacements of the MC-1 cells towards the hypoxic areas once inside the xenograft. Without magnetotactic directional guidance, only a smaller proportion of MC-1 cells that randomly swam in the direction of the xenograft could potentially be influenced by oxygen gradients in the tumoral tissues. **f**, Summary of the total average number of injected and detected MC-1 for all tumours in groups I and II. Data represent as Mean + S.D. (n = 10 for each of c, d, e, and f). Transverse tumor sections were scanned at 40× magnification and the numbers of bacteria in the tumours were estimated by image processing techniques (see Methods: MC-1 count). The results show that a significant number of the peritumorally injected MC-1 being magnetically-guided using a relatively simple static directional magnetic field was able to penetrate the xenograft, unlike for the bacteria which were not guided into the tumour. These results likely represent a simplified case scenario as many other more sophisticated modulated directional magnetic fields could be investigated to increase further the targeting ratios achieved in this study.

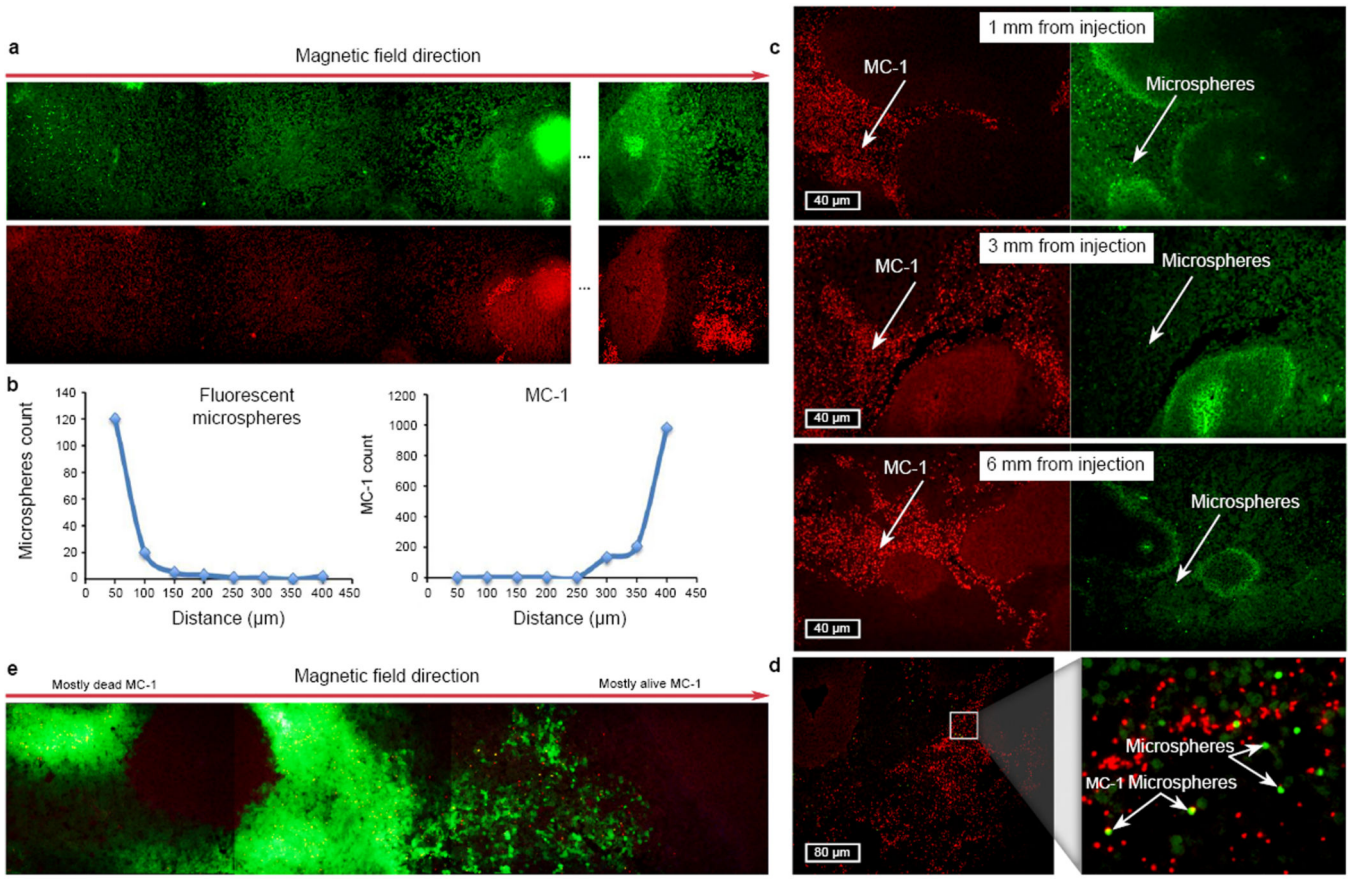

Figure 4. Superior penetration of MC-1 cells over passive diffusion in HCT116 xenografts demonstrated by two methods

(1) peritumoral injection of a mixture of MC-1 cells and similar size polymer fluorescent microspheres (**a**,**b**,**c**,**d**) and (2) peritumoral injection of a mixture of dead and live MC-1 (**e**). For both methods, the injection was followed by 30 min of magnetic guidance directed towards the centre of the tumoral volume. **a**, 20× images of MC-1 Texas red fluorescent and FITC fluorescent microspheres at various tumoral depths in a longitudinal tumour section showing the superior penetration of MC-1 cells inside the tumour. The small wide strip marks the site where the tumour slice was cut into two parts – two rectangles: one larger and one smaller. **b**, Quantity of fluorescent microspheres vs. live MC-1 at various tumoral depths related to the experiment in (**a**) and depicting the superior penetration of live MC-1 well passed the diffusion limits of the fluorescent microspheres. **c**, 20× images of MC-1 Texas red fluorescent and FITC fluorescent beads at 1, 3, and 6 mm inside the HCT116 xenograft, again showing the much higher penetration depths of the live MC-1. **d**, Co-localization of MC-1 bead complexes at a tumoral depth of 4 mm suggesting the capability of MC-1 cells to transport large therapeutic payloads deep in tumoral tissues. Dead MC-1 are unable to move in the magnetic field, and are located in the far left section, whereas the live MC-1 which typically migrate along the magnetic field are in the right section confirming that they indeed moved along the direction of the magnetic field. **e**, 20× images of live and dead MC-1 at different tumoral depths showing the superior penetration inside the tumor of live cells.

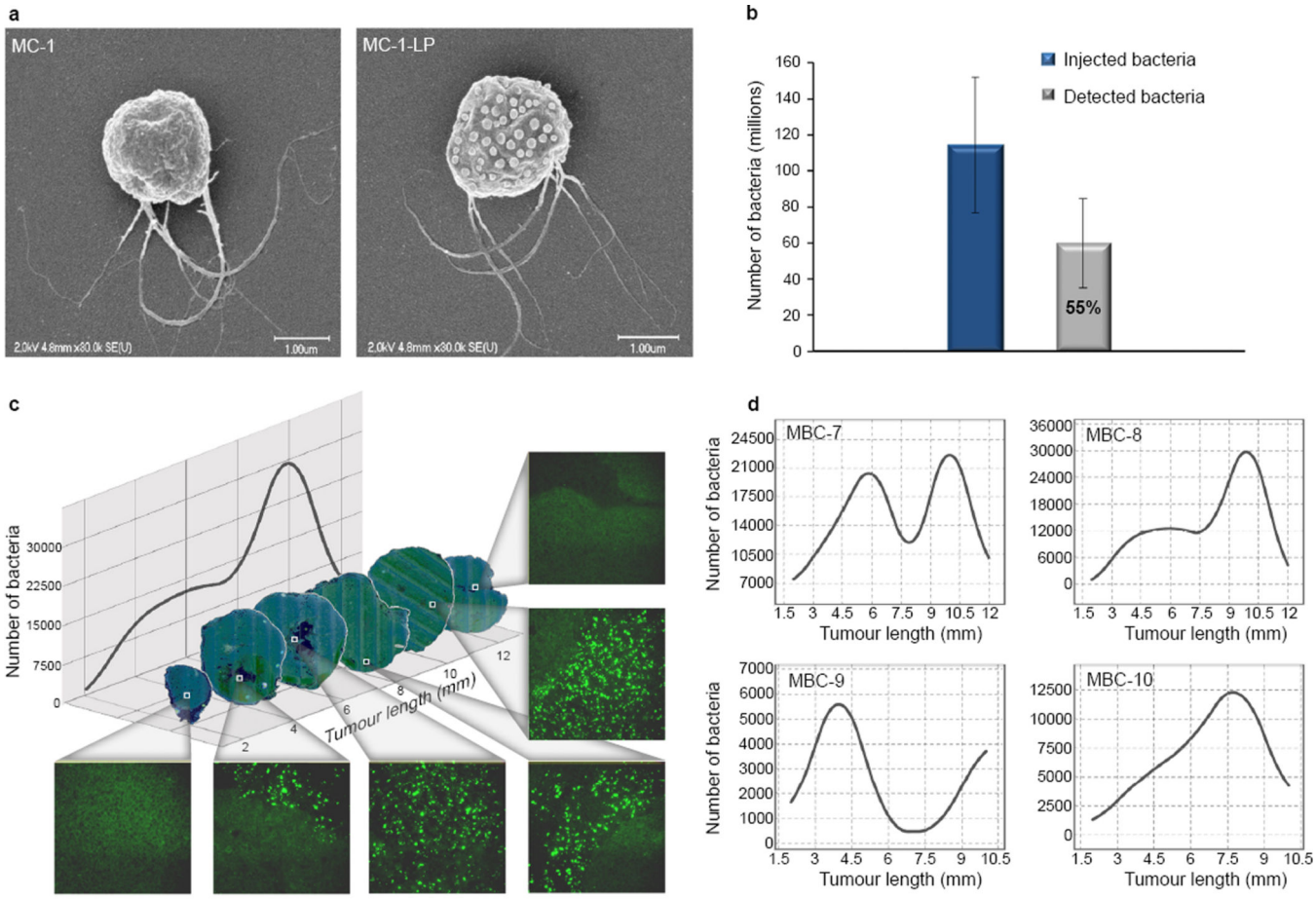

Figure 5. Targeting ratios of MC-1-LP in HCT116 xenografts

a, Scanning electron microscopy images of unloaded MC-1 vs. MC-1-LP (right) with ~70 SN-38 loaded liposomes (diam. ~170 nm) attached to the surface of each cell. **b**, Estimated mean ratios of MC-1-LP found in the tumour after targeting with a directional magnetic field. The total numbers of bacteria in the tumours were estimated by direct count of the MC-1 cells obtained from homogenization of the tumours or image processing techniques of transverse tumor sections. The data represents the mean ± S.D. (n = 10 tumours). Number of bacteria was calculated using 10 different tumours isolated from the 10 tumour-bearing mice collected in three independent experiments. Five tumours were homogenized to obtain exact count and the other five were cut into numerous sections, stained and counted. The preliminary results already show a mean targeting ratio of 55% similar to the targeting results achieved with the unloaded MC-1 under the same experimental and physiological conditions. These results suggest that the MC-1 can be loaded without significantly affecting the targeting ratios in tumours. **c**, Transverse tumour sections of MC-1-LP after targeting, images of each section were acquired using a fluorescence optical microscope equipped with a 40× magnification objective lens. The images show a good distribution of the loaded MC-1 cells throughout the tumour. **d**, Example of MC-1-LP distribution inside four different tumors. The differences in the locations of the hypoxic regions among the various xenografts lead to variations of the distributions of the loaded MC-1 between the targeted xenografts.